# *In vivo* measurements of lung function using respiratory-gated micro-computed tomography in a smoke-exposure model of chronic obstructive pulmonary disease

**Nancy L. Ford,[a,b,*] Ian Lee,[a] Julia Hwangbo,[a] Anthony Tam,[c] and Don D. Sin[c,d]**

[a]The University of British Columbia, Department of Oral Biological and Medical Sciences, Vancouver, British Columbia, Canada

[b]The University of British Columbia, Department of Physics and Astronomy, Vancouver, British Columbia, Canada

[c]The University of British Columbia, St. Paul's Hospital, Centre for Heart Lung Innovation, Vancouver, British Columbia, Canada

[d]The University of British Columbia, Division of Respirology, Department of Medicine, Vancouver, British Columbia, Canada

## Abstract

**Purpose:** We hypothesize that *in vivo* respiratory-gated micro computed tomography (micro-CT) imaging can noninvasively provide structural and functional information about the lungs in a cigarette-exposure model of chronic obstructive pulmonary disease in mice.

**Approach:** Female C57BL/6 mice were exposed to cigarette smoke or ambient air for 1, 3, or 6 months. Each mouse received a respiratory-gated micro-CT scan at baseline and another scan following the exposure period, while anaesthetized and free-breathing. Images were obtained representing end-expiration and peak inspiration, and measurements were performed to characterize the lung structure and compute functional metrics. Following the final micro-CT session, the mice were euthanized and the lungs prepared for histology.

**Results:** Following 6 months of smoke-exposure, the mice exhibited larger increases in end-expiration lung volume and functional residual capacity, and a reduction in weight gain when compared with air-exposed mice. The histogram of CT numbers in the lung obtained during end-expiration also showed a shift to lower CT numbers following 6 months of smoke-exposure, indicating increased air content within the lungs. The metrics suggested air-trapping in the lung, which is consistent with emphysema. In the 3-month exposure group, only the reduction in weight gain was significant compared with the air-exposed group. Histological analysis confirmed that the 6-month smoke-exposed mice likely developed centrilobular emphysema as measured by the mean linear intercept.

**Conclusions:** Respiratory-gated micro-CT imaging of free-breathing mice at multiple respiratory phases is noninvasive and provides additional information about lung structure and function that complements postmortem techniques and could be used to monitor changes over time.

*Address all correspondence to Nancy L. Ford, nlford@dentistry.ubc.ca

## 1 Introduction

Smoking tobacco cigarettes has been a known health hazard since the late 1950s.[1] Smoking is a risk factor for numerous respiratory and cardiovascular conditions that lead to serious diseases and mortality. Two main respiratory health concerns arising from smoking are lung cancer, due to the inhalation of toxins and exposure of carcinogenic by-products of combustion, and chronic obstructive pulmonary disease (COPD), which is associated pathologically with inflammation, gas trapping, and emphysema, along with remodeling of the small airways and pulmonary vasculature.

To investigate the disease pathogenesis of COPD *in vivo* requires modeling in rodents. Models have emerged using guinea pigs[2,3] and mice[4–11] with COPD being induced by exposure to the chemicals found in cigarette smoke over a period of up to six months. In guinea pigs, histological analysis has demonstrated that airway remodeling and emphysema can be stopped or slowed by treatment with a myeloperoxidase inhibitor,[2] which also prevents the muscularization of small intrapulmonary arteries. Wright et al. reported the use of a guinea pig model to investigate smoke-induced pulmonary hypertension, endothelial dysfunction, emphysema and small airway remodeling.[3] Mouse models have shown pulmonary inflammation as measured by histology and in bronchoalveolar lavage.[7,8]

To investigate the lungs in 3D, high-resolution micro computed tomography (micro-CT) can be used on fixed specimens, and *in vivo* micro-CT machines can image live rodents. To investigate the lungs at a specified respiratory phase, prospectively gated imaging allows for each projection view to be acquired at the same point in the respiratory cycle,[12–16] whereas retrospective approaches select only the desired in-phase projections for reconstruction.[17–22] Parameswaran et al.[5] fixed sections of mouse lung tissue and stained with silver to provide contrast in the micro-CT images in order to measure the alveolar airspace volume. Using an *in vivo* micro-CT scanner, the lung volume, CT density, and low attenuation regions can be quantified in live animals.[4,9,11] Recent papers have reported using respiratory-gated[10] or respiratory- and cardiac-gated micro-CT imaging[6] during the end expiratory phase to improve the measurements of air trapping. Other researchers have used *in vivo* micro-CT imaging to study emphysema in a knock-out model[23] or in an elastase-exposure model.[24,25]

The majority of recent studies discussed here focus on either the small airway remodeling in excised tissue or on the low attenuation regions and gas trapping *in vivo* as markers of emphysema. To further understand COPD and how this disease progresses, longitudinal *in vivo* studies of the airways, lung function, and pulmonary vasculature together using noninvasive 3D imaging will become necessary. In this paper, we perform longitudinal *in vivo* micro-CT in mice that had been exposed to cigarette smoke for different durations up to six months. The micro-CT images will provide anatomical and functional measurements of the lungs and airways and will be correlated with histological assessment of the excised lung tissues.

## 2 Methods

### 2.1 *Animal Model and Study Design*

All animal experiments were conducted under animal care guidelines following institutional ethical review by the University of British Columbia Animal Care Committee (approval #A17-0320) and in accordance with the Canadian Council on Animal Care guidelines. Female C57BL/6 mice ($N = 60$) were obtained (Jackson Laboratory, Sacramento, California) and assigned to a smoking or control group. Throughout the experiment, the mice lived in group housing and were fed *ad libitum*. Once the mice were 9-weeks old, exposure experiments were initiated. Power calculations were performed using data from previous studies, with 12 mice per exposure group expected to have 80% power for volumetric measurements with an expected difference of 0.04 mL and a standard deviation of 0.03 mL. For the control mice, we reduced the number of mice to 8 per group, as previous CT imaging studies in healthy mice have showed good consistency for age-matched and sex-matched mice.

Micro-CT images were taken 4 to 6 days pre-exposure (baseline). Air-exposed mice ($N = 24$) remained in their cages over a 1-, 3-, or 6-month period where they breathed ambient

room air (8 mice for each exposure period). Smoke-exposed mice ($N = 36$) were subjected to daily 1.5-h exposure sessions, 5 days per week, for either 1, 3, or 6 months (12 mice per exposure period). Kentucky research cigarettes (Center for Tobacco Reference Products, Lexington, Kentucky) were used as described previously.[26,27] Micro-CT images were repeated 3 to 4 days following the last exposure session (endpoint). The mice were then euthanized, and the lungs were excised and formalin-fixed for histology.

## 2.2 Micro-CT Imaging

Mice were anesthetized in an induction chamber (5% isoflurane in $O_2$) until unresponsive to toe pinch and maintained with 1.5% to 2% isoflurane via a nose-cone. Each mouse received an iodinated blood-pool contrast agent (Fenestra VC, Medilumine, Montreal, Canada) via a tail vein injection at a dosage of 0.01 mL Fenestra VC per gram body weight. The micro-CT images were obtained using the eXplore CT120 (Trifoil Imaging, Chatsworth, California) using a respiratory-gated protocol (80 kV, 40 mA, 0.3 Gy, 210 projections with 100 ms exposures). A Biovet physiological monitoring system (m2m Imaging, Cleveland, Ohio) was used to trigger image acquisition, as described previously.[13] A pneumatic cushion, positioned between the mouse and scanning bed and aligned with the diaphragm, measured and displayed the respiratory signal on a laptop computer. Trigger points were selected near the end of inhale and used by the micro-CT scanner to initiate the x-ray projection image (inspiration), and a second triggered acquisition 150 to 450 ms later to align with the expiratory phase (most images used 300 to 400 ms delay times). Scanning sessions varied in duration due to variations in individual respiratory rates ($\sim$20 min). Images were collected during inspiration and end expiration and reconstructed with 0.075 mm isotropic voxel spacing.

## 2.3 Histology

Following the final micro-CT imaging session, the mice were euthanized with an overdose of ketamine (300 mg/g) and xylazine (20 mg/g) delivered intraperitoneally. Histological slides (2/mouse) were prepared for a subset of the mice, $n = 5$ for 1-month, $n = 7$ for 3-month and $n = 6$ for 6-month air-exposed mice, and for $n = 7$ for 1-month and 3-month and $n = 11$ for 6-month smoke-exposed mice. The lungs were excised from the thorax and were inflation-fixed by instillation of 10% formalin at 30 cm $H_2$0 to allow the alveolar structures to unfold, and submerging the lungs in 10% formalin for at least 24 h to ensure complete fixation. The lungs were paraffin-embedded and cut into coronal sections (5 $\mu$m) with a microtome to allow for both left and right lungs to be present on the same slide and to increase the sampling coverage of the organ. Tissue sections were deparaffinized and dehydrated in ethanol, then stained with hematoxylin and eosin (H&E) for histopathological assessment of mean linear intercept (Lm), and Masson's Trichrome for assessment of the total airway collagen. All of the sections were mounted onto glass slides and imaged using the Aperio slide scanning microscope (Leica Biosystems, Concord, Ontario, Canada) at 13.1× magnification.

## 2.4 Data Analysis

MicroView (Trifoil Imaging, Chatsworth, California) was used to perform image-based analysis of the micro-CT images, as described previously.[28] A threshold-based seeded region-growing algorithm was used to perform volumetric measurements of the lungs and major airways at both respiratory phases, beginning 2 mm above the carina and extending to the full extent of the lungs. The thresholds were selected using Otsu's method[29] to identify the HU value that separated the lung from the surrounding tissue (0 HU) and to separate the major airways from the rest of the lung (−900 HU). For consistency, the same threshold values were applied to all images. Once the desired anatomy was segmented, the segmented volume and mean CT number were recorded. Histograms were plotted over the range 0 HU to −1050 HU with a bin size of 50 HU to compare the distribution of gray-scale values.

The volumetric measurements were combined to determine the functional residual capacity (FRC), tidal volume (Vt), and the low attenuation area (LAA). The FRC and Vt were corrected

for the fractional air content instead of simply subtracting the segmented volumes as given in Eqs. (1) and (2),[28] where the volumes and mean CT densities were measured in the micro-CT images, and the CT density$_{air}$ is the theoretical value for air and is set to $-1000$ HU:

$$\text{FRC(mL)} = \text{volume}_{\text{expiration}} * \frac{\text{mean CT density}_{\text{expiration}}}{\text{CT density}_{\text{air}}} \tag{1}$$

$$\text{Vt(mL)} = \text{volume}_{\text{inspiration}} * \frac{\text{mean CT density}_{\text{inspiration}}}{\text{CT density}_{\text{air}}} - \text{FRC}. \tag{2}$$

The LAAs were identified as voxels with a CT number less than $-950$ HU using the histograms of the inspiration images. The volume of these areas was measured and the %LAA is the ratio between the low attenuation to the full lung volume at inspiration:

$$\%\text{LAA} = \frac{\text{volume}_{<-950}}{\text{volume}_{\text{inspiration}}}. \tag{3}$$

The inspiratory capacity to total lung capacity ratio (IC/TLC) is not possible to measure in anesthetized free-breathing mice since they are not able to intake maximal inspiration on demand. Instead, we present the Vt to resting inspiratory (RI) volume using the resting volumes in place of maximal volumes:

$$\%\frac{\text{Vt}}{\text{RI}} = \frac{\text{Vt}}{\text{FRC} + \text{Vt}}. \tag{4}$$

Histological analysis was performed using the ImageScope (Leica Biosystems, Concord, Ontario, Canada) software according to standard methods.[30] From the H&E stained slides, the number of intercepts from 18 to 25 randomly located line lengths (line length of 1000 $\mu$m) was counted:

$$\text{Lm} = 2 \times \frac{\text{total line length in } \mu\text{m}}{\text{total \# of intercepts}}. \tag{5}$$

From the slides stained with Masson's Trichrome, collagen expression was assessed by measuring the amount of green color on the slides. Total airway collagen intensity from 15 to 20 random airways per slide was calculated by normalizing the collagen signal (green color) to the basement membrane (BM) length:

$$\text{total airway collagen intensity} = \frac{\text{(collagen signal)}}{\text{BM length}}. \tag{6}$$

Statistical analysis was performed using Prism (9.1.2, GraphPad Software, La Jolla, California). Outliers were identified using a Grubbs test and removed from the analysis (maximum of 1 outlier per exposure group). To analyze the micro-CT and histology measurements, one-way ANOVA with Sidak *post hoc* test was performed between smoke-exposed and age-matched air-exposed groups ($\alpha = 0.05$).

## 3 Results

Images of a representative mouse from each time point of the smoke-exposed group are shown in Fig. 1, along with a baseline image. These images were obtained during end-expiration. Note the air-filled regions in the lungs appear darker following 6 months of smoke-exposure [Figs. 1(c) and 1(g)] compared with the shorter exposure durations. The mean CT numbers for these mice were $-288$ HU for the 1-month exposure [Figs. 1(a) and 1(e)], $-253$ HU for the 3-month exposure [Figs. 1(b) and 1(f)], $-351$ HU for the 6-month exposure [Figs. 1(c) and 1(g)], and $-267$ HU for the baseline images [Figs. 1(d) and 1(h)]. Figure 2 shows segmentations of the lung (below 0 HU), the mean attenuation (below $-600$ HU), and the low attenuation
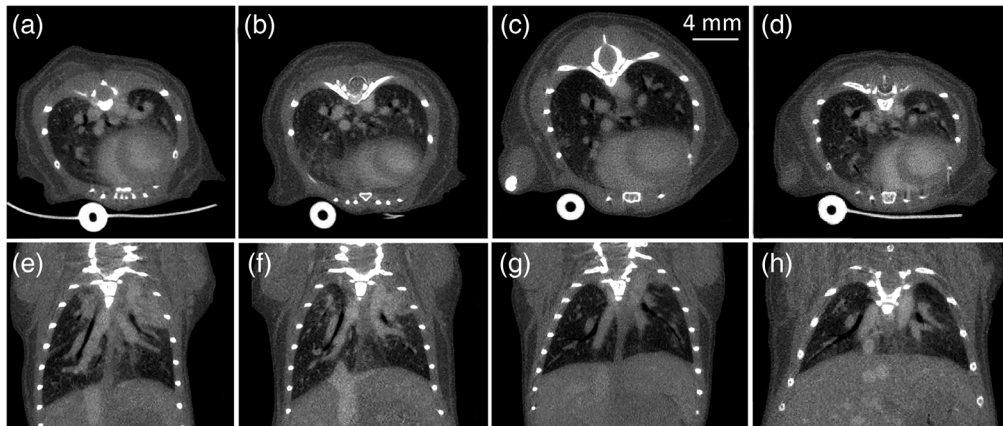
**Fig. 1** Axial (top) and coronal (bottom) slices from images taken following (a), (e) 1 month; (b), (f) 3 months; and (c), (g) 6 months of smoke-exposure. (d), (h) Baseline images for the same mouse as the 6-month exposure. Images were obtained during end-expiration and reconstructed with 0.075-mm voxel spacing.
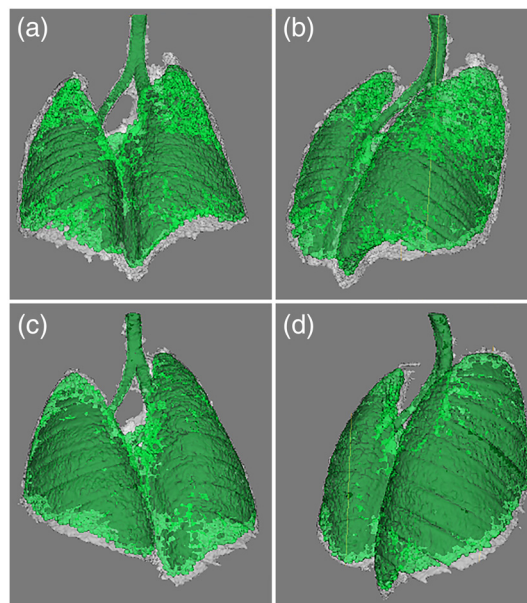


**Fig. 2** Segmentations of the lung in white, average attenuation regions (below −600 HU) in green and low attenuation regions (below −900 HU) in dark green from inspiration images taken following (a), (b) 6 months of smoke-exposure and (c), (d) 6 months of air-exposure. The air-exposed mouse has a more uniform distribution of the low attenuation regions compared with the smoke-exposed mouse.

(below −900 HU) in the inspiration phase. The top row shows the smoke-exposed mouse and the bottom row shows an age-matched air-exposed mouse looking from the sternum and from the right side of the animal. The uneven distribution of gray scale values shows the patchy regional inhomogeneities in the lung ventilation that is typical in COPD.

Measurements of the lung and major airway volumes, and the corresponding lung and major airway densities were made in the baseline and endpoint images for both respiratory phases, whereas the %LAA was measured in the inspiration images only (Table 1). The measurements from the two respiratory phases were combined to calculate the functional metrics: Vt, FRC, and Vt/RI ratio (Table 2). Statistically significant differences between baseline and endpoint are shown in bold font for both tables. During inspiration, both the smoking and control mice

**Table 1** Volumetric measurements and CT densities measured before and after the exposures. Mean and standard deviations for the lung volume, lung density, major airway volume, and % LAAs.

| Inspiration | Lung volume (mL) | P-value | Lung CT density (HU) | P-value | Major airway volume (µL) | P-value | %LAA (%) | P-value |
|---|---|---|---|---|---|---|---|---|
| 6M Smoking: B | **0.64 ± 0.09** | **<0.0001** | −526 ± 76 | 0.9994 | 45.0 ± 65.4 | 0.6352 | 6.13 ± 6.4 | 0.0601 |
| 6M Smoking: E | **0.87 ± 0.06** | | −515 ± 48 | | 20.1 ± 20.7 | | 2.28 ± 1.6 | |
| 6M Control: B | **0.56 ± 0.06** | **<0.0001** | −512 ± 83 | 0.9994 | 2.31 ± 0.27 | 0.6688 | 2.70 ± 3.3 | 0.9299 |
| 6M Control: E | **0.76 ± 0.06** | | −525 ± 68 | | 37.7 ± 62.0 | | 4.39 ± 4.5 | |
| 3M Smoking: B | **0.59 ± 0.05** | **0.0033** | −519 ± 57 | 0.9733 | 17.3 ± 15.9 | >0.9999 | 2.36 ± 1.7 | >0.9999 |
| 3M Smoking: E | **0.71 ± 0.06** | | −497 ± 52 | | 18.9 ± 18.3 | | 2.42 ± 1.9 | |
| 3M Control: B | **0.57 ± 0.13** | **<0.0001** | −466 ± 120 | 0.0513 | 31.0 ± 54.5 | 0.1010 | 4.54 ± 6.1 | 0.9178 |
| 3M Control: E | **0.76 ± 0.12** | | −557 ± 54 | | 81.2 ± 71.7 | | 6.29 ± 2.1 | |
| 1M Smoking: B | **0.55 ± 0.06** | **0.0003** | −486 ± 94 | 0.1253 | 4.62 ± 4.2 | 0.0838 | 2.15 ± 2.5 | 0.1329 |
| 1M Smoking: E | **0.68 ± 0.09** | | −551 ± 18 | | 48.9 ± 28.3 | | 5.54 ± 2.1 | |
| 1M Control: B | 0.56 ± 0.05 | 0.2157 | −500 ± 50 | 0.1152 | **6.50 ± 6.3** | **0.0054** | **1.55 ± 0.8** | **0.0007** |
| 1M Control: E | 0.64 ± 0.08 | | −580 ± 43 | | **77.7 ± 56.5** | | **8.60 ± 4.4** | |

**Table 1** (*Continued*).

| Inspiration | Lung volume (mL) | P-value | Lung CT density (HU) | P-value | Major airway volume (µL) | P-value | %LAA (%) | P-value |
|---|---|---|---|---|---|---|---|---|
| Expiration | | | | | | | | |
| 6M Smoking: B | **0.35 ± 0.06** | **<0.0001** | **−293 ± 52** | **0.0303** | **1.95 ± 0.70** | **<0.0001** | | |
| 6M Smoking: E | **0.60 ± 0.05** | | **−347 ± 32** | | **3.10 ± 0.56** | | | |
| 6M Control: B | **0.35 ± 0.05** | **0.0002** | −316 ± 71 | 0.9996 | **1.83 ± 0.54** | **0.0035** | | |
| 6M Control: E | **0.47 ± 0.07** | | −323 ± 68 | | **2.78 ± 0.64** | | | |
| 3M Smoking: B | 0.38 ± 0.04 | 0.2103 | −307 ± 15 | 0.1598 | 1.68 ± 0.30 | 0.2655 | | |
| 3M Smoking: E | 0.43 ± 0.05 | | −267 ± 33 | | 2.12 ± 0.67 | | | |
| 3M Control: B | 0.37 ± 0.06 | 0.2288 | −305 ± 22 | >0.9999 | **2.00 ± 0.36** | **0.0001** | | |
| 3M Control: E | 0.43 ± 0.07 | | −308 ± 48 | | **2.44 ± 0.61** | | | |
| 1M Smoking: B | 0.32 ± 0.07 | 0.0479 | −288 ± 42 | >0.9999 | 1.55 ± 0.44 | 0.4735 | | |
| 1M Smoking: E | 0.38 ± 0.07 | | −287 ± 30 | | 1.91 ± 0.42 | | | |
| 1M Control: B | 0.37 ± 0.07 | 0.9992 | −316 ± 52 | >0.9999 | 2.00 ± 0.36 | 0.4580 | | |
| 1M Control: E | 0.36 ± 0.05 | | −310 ± 38 | | 2.45 ± 0.61 | | | |

Note: B, baseline scans; E, endpoint scans; 6M, 6 months; 3M, 3 months; and 1M, 1-month exposure times.

**Table 2** Functional metrics measured before and after the exposures. Mean and standard deviations for body weight, FRC, Vt, and the ratio of Vt to RI volume (Vt/RI).

| | Weight (g) | P-value | FRC (mL) | P-value | Vt (mL) | P-value | Vt/RI (%) | P-value |
|---|---|---|---|---|---|---|---|---|
| **Smoke-exposed** | | | | | | | | |
| 6M baseline | **19.8 ± 1.2** | **<0.0001** | **0.11 ± 0.03** | **<0.0001** | 0.23 ± 0.06 | >0.9999 | **70.6 ± 4.6** | **<0.0001** |
| 6M endpoint | **23.3 ± 1.4** | | **0.21 ± 0.03** | | 0.24 ± 0.05 | | **51.4 ± 3.8** | |
| 3M baseline | **19.5 ± 1.3** | **0.0112** | 0.12 ± 0.01 | >0.9999 | 0.19 ± 0.05 | 0.2333 | 63.3 ± 9.2 | 0.7575 |
| 3M endpoint | **21.4 ± 0.8** | | 0.12 ± 0.02 | | 0.24 ± 0.05 | | 67.5 ± 5.3 | |
| 1M baseline | 19.4 ± 1.3 | >0.9999 | 0.09 ± 0.03 | 0.6818 | **0.17 ± 0.06** | **0.0039** | 63.6 ± 7.1 | 0.1924 |
| 1M endpoint | 19.5 ± 1.5 | | 0.11 ± 0.03 | | **0.25 ± 0.05** | | 70.9 ± 4.1 | |
| **Air-exposed** | | | | | | | | |
| 6M baseline | **18.9 ± 1.5** | **<0.0001** | **0.11 ± 0.04** | **0.0296** | 0.16 ± 0.02 | 0.0537 | 61.9 ± 6.5 | >0.9999 |
| 6M endpoint | **26.3 ± 2.6** | | **0.16 ± 0.05** | | 0.24 ± 0.06 | | 61.1 ± 9.8 | |
| 3M baseline | **19.6 ± 0.7** | **<0.0001** | 0.11 ± 0.02 | 0.6360 | **0.17 ± 0.13** | **0.0004** | **52.8 ± 19.9** | **0.0012** |
| 3M endpoint | **24.8 ± 2.4** | | 0.14 ± 0.04 | | **0.29 ± 0.07** | | **68.7 ± 5.1** | |
| 1M baseline | 18.7 ± 0.7 | 0.5944 | 0.12 ± 0.04 | 0.9981 | **0.16 ± 0.02** | **0.0066** | **58.1 ± 8.8** | **0.0313** |
| 1M endpoint | 19.8 ± 1.1 | | 0.11 ± 0.03 | | **0.26 ± 0.05** | | **69.7 ± 5.2** | |

Note: 6M, 6 months; 3M, 3 months; and 1M, 1-month exposure times.

**Table 3** Change in lung measurements from baseline to endpoint: mean and standard deviations for changes in lung and major airway volumes, and the corresponding CT density taken during end expiration (top) and inspiration (bottom). The % LAA is also given during inspiration. Values are the endpoint measurements minus baseline for the same mouse, averaged for the group. Bold entries indicate statistically significant differences between the smoke-exposed and age-matched air-exposed mice.

| | 6 Month | | | 3 Month | | | 1 Month | | |
|---|---|---|---|---|---|---|---|---|---|
| Expiration | Smoke | Air | P-value | Smoke | Air | P-value | Smoke | Air | P-value |
| Lung volume (mL) | **0.25 ± 0.05** | **0.13 ± 0.05** | **0.0025** | 0.05 ± 0.07 | 0.06 ± 0.07 | 0.9873 | 0.06± 0.11 | −0.01 ± 0.07 | 0.0848 |
| Lung density (HU) | −53.0 ± 44.3 | −36.3 ± 42.4 | 0.8485 | 32.3 ± 56.0 | −3.1 ± 42.3 | 0.2840 | 0.1 ± 49.2 | 5.4 ± 39.6 | 0.9952 |
| Major airway volume (µL) | 1.16 ± 0.64 | 0.95 ± 0.81 | 0.8895 | **0.34 ± 0.72** | **1.19 ± 0.67** | **0.0251** | 0.36 ± 0.59 | 0.45± 0.66 | 0.9894 |
| Inspiration | | | | | | | | | |
| Lung volume (mL) | 0.21 ± 0.05 | 0.20 ± 0.07 | 0.9978 | 0.10 ± 0.11 | 0.18 ± 0.05 | 0.1476 | 0.16 ± 0.13 | 0.08 ± 0.08 | 0.2234 |
| Lung density (HU) | 10.7 ± 97.4 | −12.7 ± 87.9 | 0.9154 | **22.2 ± 68.4** | **−90.2 ± 77.7** | **0.0179** | −48.6 ± 112.6 | −61.7 ± 19.0 | 0.9841 |
| Major airway volume (µL) | −0.03 ± 0.08 | −0.02 ± 0.03 | 0.9651 | 0.00 ± 0.02 | 0.05 ± 0.10 | 0.2178 | 0.04 ± 0.03 | 0.07 ± 0.06 | 0.4928 |
| LAA (%) | −4.3 ± 7.2 | −0.4 ± 5.7 | 0.2919 | 0.0 ± 2.1 | 3.4 ± 6.5 | 0.4193 | 2.6 ± 3.6 | 7.0 ± 4.3 | 0.1706 |

exhibited significant increases in lung volume for the 6-month ($p < 0.0001$ for both) and 3-month ($p = 0.0033$ for smoking and $p < 0.0001$ for control) exposure groups. The 1-month smoked-exposed mice also showed increased lung volume ($p = 0.0003$), whereas the control group showed an increase in major airway volume ($p = 0.0054$) and %LAA ($p = 0.0007$), which may be due to the small volumes measured at baseline. The 6-month exposure groups were the only groups to show a significant increase in FRC ($p < 0.0001$ for smoking and $p = 0.0296$ for control). The 6-month smoking group was the only group with no change in Vt and a decrease in Vt/RI.

To account for the biological variability and the growth of the mice during the study, the metrics we compared were the changes over the course of the exposure period (endpoint to baseline), where positive changes indicate an increase over the exposure period and negative values indicate a reduction in the measurements over the exposure period. The changes in the measured values are given in Table 3, with bold font indicating statistically significant differences between the smoke-exposed and air-exposed mice for the same exposure duration. The 6-month smoke-exposure group showed a significantly larger increase in lung volume at end expiration ($p = 0.0025$) than age-matched controls. The 3-month smoke-exposed mice showed an increase in the air content in the lungs during inspiration ($p = 0.0198$) and an increase in the major airway volume during end expiration ($p = 0.0251$). The changes in the calculated functional metrics (endpoint to baseline), along with body weight, are plotted as Fig. 3, with the $p$-values included on the plot. The histograms for inspiration and expiration are shown in Fig. 4, with the baseline values shown as squares, and the endpoint values as circles. Each data point is the mean value for the exposure group with the standard error in the mean shown as errorbars. From these curves, there is a lot of overlap between the groups. The 6-month smoke-exposed group (green) shows a deviation to higher counts and lower CT #, indicating that there is increased air in the lung at both respiratory phases. This increased air is consistent with air-trapping, a clinical sign of COPD.

Measurements on the histological slides were completed for air-exposed mice with $n = 5$ for 1-month, $n = 7$ for 3-month, and $n = 6$ for 6-month exposure, and for smoke-exposed mice with $n = 7$ for 1-month and 3-month and $n = 11$ for 6-month exposures. Sample images from each
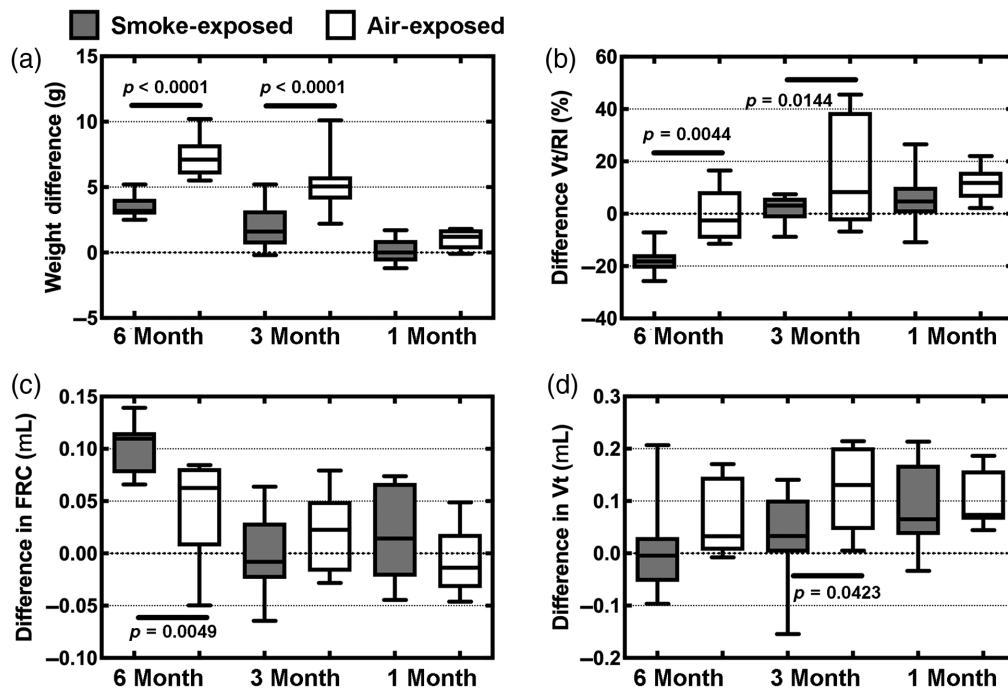


**Fig. 3** Mean differences between the baseline and endpoint scans showing the changes in (a) body weight, (b) ratio of Vt/RI, (c) FRC, and (d) Vt. *P*-values are shown for comparisons between smoke-exposed and air-exposed mice. Vt, tidal volume; RI, resting inspiration; and FRC, functional residual capacity.
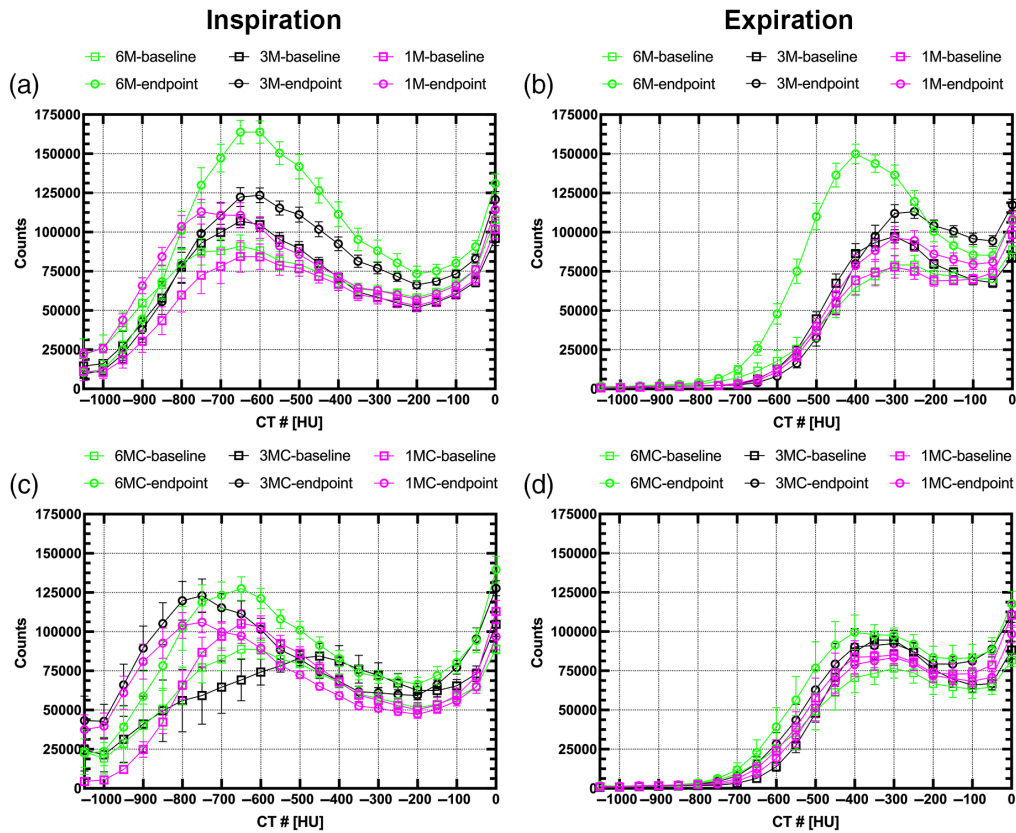
**Fig. 4** Histograms of the CT number in Hounsfield units within the lungs. The curves show the mean and standard error for the baseline images (squares) and the endpoint images (circles). The smoke-exposed mice are shown during (a) inspiration and (b) expiration, and the air-exposed mice during (c) inspiration and (d) expiration.

exposure group are shown in Fig. 5 for H&E staining, which demonstrates airway disruptions for the smoke-exposed mice starting at 3 months. Airway disruptions are a degradation of the lung tissue, which indicates emphysema and air trapping in the lungs. Although the volumetric measurements done in the CT images are not sensitive enough to pick up the early stage changes in the lung, the 6-month smoke exposure group shows air-trapping, which is consistent with the histological results. The mean linear intercept is shown in Fig. 5(d), with a statistically significant difference observed between the air-exposed and smoke-exposed mice following the 6-month exposure time. Figure 6 shows collagen in a representative airway stained with Masson's Trichrome. Plots are shown in Fig. 6(d) for the total collagen intensity, with no significant differences found between the groups. Measurements were performed in the peripheral airways, with airway diameters down to 200 $\mu$m. The histological results are consistent with other studies,[2,26,31] which confirms that the smoke-exposures were successful in inducing the COPD model as desired.

Outlier assessment using the Grubbs identified a few outliers (no more than 1 per exposure group) for a few of the measurements. These outliers were mainly a result of artifacts in the image. For a couple of scans, we noted some dark ring artifacts that were unfortunately located over the lung that we were unable to exclude from the analysis. In other images, we had a few streak artifacts caused by changes in the respiratory pattern during the scan. Eliminating these as outliers improved the confidence in the measured values as representing the organ or tissue of interest.

## 4 Discussion

The mice were quite young at the beginning of the exposure, and therefore still growing, especially over the first couple of months. The young age at initiation of exposure mimics the human
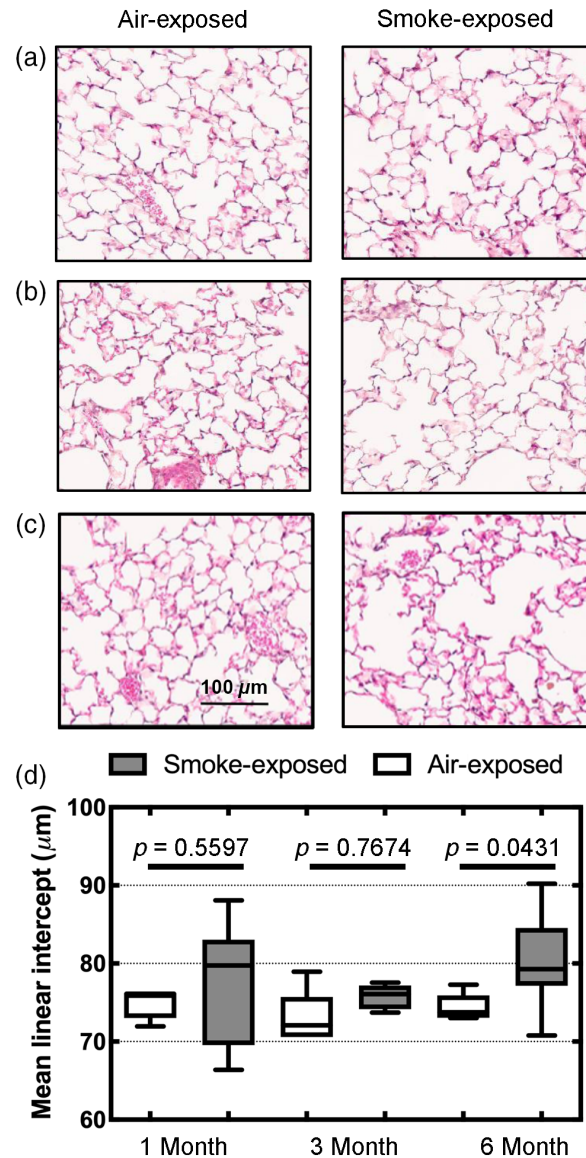
**Fig. 5** H&E stained slides for air-exposed and smoke-exposed mice following exposures of (a) 1 month, (b) 3 months, (c) 6 months. (d) Plot of mean linear intercept. *P*-values are shown for comparisons between smoke-exposed and air-exposed mice.

use of cigarettes, where smoking often begins in adolescence. As a result of the mice continuing to develop during the early stage of the exposures, the measured values obtained from the micro-CT imaging data were somewhat skewed when compared to the baseline scans, as increased measured values were due to both age-related growth and to the exposure received. To account for the age-related growth, we only compared age-matched animals and to account for biological variation in animal size, we measured the change in each metric relative to baseline for individual mice to promote consistency in the data.

We found significant reductions in weight gain for the smoke-exposed mice compared with air-exposed mice following 3 or 6 months of exposure ($p < 0.0001$). All mice gained weight, but the smoke-exposed mice gained less weight than their air-exposed counterparts. As the duration of smoke-exposures increased, the weight gain was reduced.

The change in the lung volume measurements during end-expiration was increased in the 6-month smoke-exposed mice compared to air-exposed mice ($p = 0.0025$). This pattern was also seen in the FRC measurements, with smoke-exposed mice exhibiting a larger increase in FRC than can be expected by age-related growth alone ($p = 0.0049$). The change in the
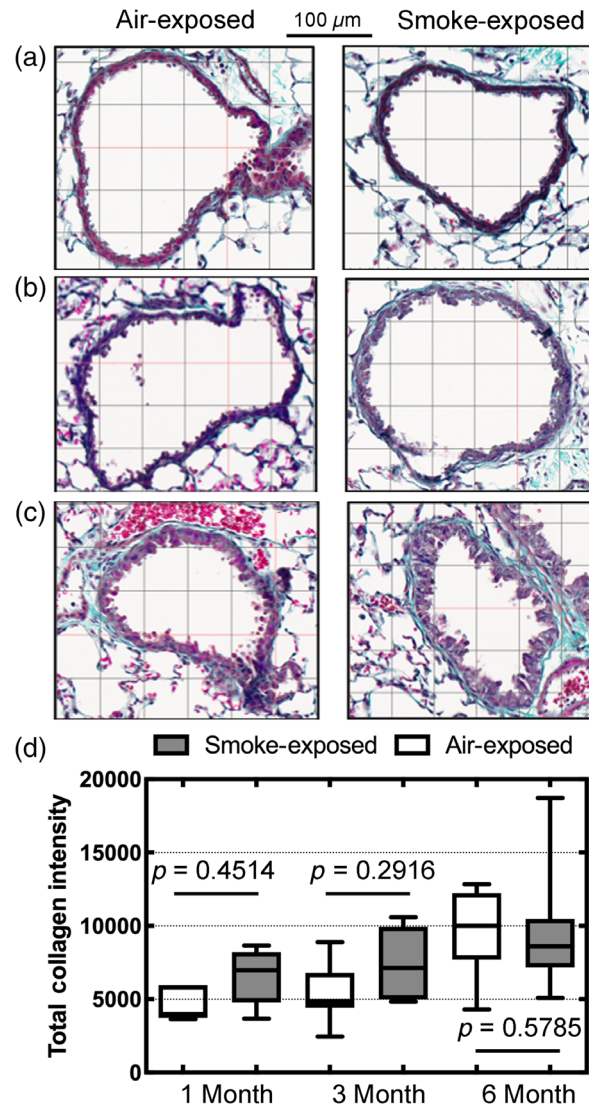
**Fig. 6** Trichrome stained slides for air-exposed and smoke-exposed mice following exposures of (a) 1 month, (b) 3 months, (c) 6 months. (d) Plot of total collagen intensity. *P*-values are shown for comparisons between smoke-exposed and air-exposed mice.

Vt/RI ratio in the 6-month smoke-exposed mice was significantly reduced compared to the air-exposed mice ($p = 0.0044$). The histogram analysis of the air content in the lungs also showed an increase in air content for the 6-month smoke-exposed animals for both respiratory phases and a noticeable shift in the peak of the curve during expiration. Together, these metrics (lung volume during end-expiration, FRC, Vt/RI, and histogram) suggest air-trapping in the lung likely related to emphysema and/or airway remodeling. Furthermore, the increase in Lm in the mice exposed for 6 months to cigarette smoke is consistent with measurements reported by Zhou et al.[32] Histological images of the 6-month time point show a similar pattern of centrilobular emphysema in published studies.[31]

The image-based measurements obtained from the micro-CT scans are whole-organ measurements, similar to the types of analyses previously published.[6,23,25] One novel aspect of this study is the inclusion of both end-expiration and peak inspiration images and the use of free-breathing animals, which allows for estimates of lung function. The functional micro-CT measurements given here are similar to what is performed in the clinical evaluation of COPD. However, the inspiratory to total lung capacity (IC/TLC) metric that is used clinically is underestimated in anaesthetized and free-breathing mice, as we can only measure the average

inhalation during tidal breathing, not the maximum inhalation, for the IC measurement. As a surrogate, we tabulated the Vt to resting inspiration ratio (Vt/RI) instead and showed significant differences in the exposure groups at 6 months.

Limitations to this study include the ability to compare directly with functional metrics obtained using other methods, such as pulmonary function testing with a ventilator. Using a ventilator would enable the researcher to fill the lungs to the inspiratory capacity and make accurate measurements of the total lung capacity. Forcing the lungs to the total lung capacity provides more information about tissue elasticity, respiratory resistance, etc., that are not possible using free-breathing mice. Furthermore, metrics that are used clinically, such as the IC/TLC can be estimated, providing a more direct linkage between preclinical studies and patient outcomes. However, this maneuver requires intubation and mechanical ventilation of the mouse, which can lead to damage and inflammation in the trachea or overinflation of the lungs[33] that will result in measured volumes that are over-estimated in the micro-CT images.

The 1-month and 3-month exposure groups did not show significant differences for metrics related to COPD. The development of COPD is not uniform throughout the lung parenchyma. Since the micro-CT metrics FRC, Vt, %LAA, and Vt/RI are based on whole-lung measurements, small regional changes may be lost. In reality, the smoke-exposures may not induce measurable effects until later time points, which have been suggested in the literature[8,32] for histological measurements. Some COPD metrics were identified for the 6-month exposure group, which suggests that *in vivo* micro-CT imaging is sensitive to these markers.

This study represents the first *in vivo* functional micro-CT imaging study of smoke-exposed mice with different exposure durations. Although other researchers have published micro-CT studies of smoke-induced or elastase-induced emphysema, they focused on a single phase in the respiratory cycle,[6,10] or were ungated,[4,9,11] or used breath-hold during the scans.[24,25] Images taken from a single respiratory phase can only assess lung volume and air content at that phase, so functional information is lost, whereas ungated images provide an average lung size and air content over the full cycle. Breath-hold imaging can be done at multiple phases, but the lungs of rodents are often over-inflated during mechanical ventilation,[33] so any functional information will suffer from a systematic error. By performing the micro-CT imaging at multiple phases in the cycle in free-breathing mice, as described in this study, we can add important functional metrics, such as Vt and Vt/RI ratio, to the analysis.

In this study, we demonstrate that *in vivo* respiratory-gated micro-CT obtained at multiple respiratory phases can provide information about the lung structure and function of free-breathing mice in a model of COPD. This noninvasive technique will allow preclinical researchers to use imaging techniques consistent with the clinical diagnosis of COPD, image mice at multiple time points within a study, and will enable further research to assess new therapeutic treatments *in vivo*.

## Disclosures

The authors have no conflicts of interest.

## Acknowledgments

## References

1. R. N. Proctor, "The history of the discovery of the cigarette-lung cancer link: evidentiary traditions, corporate denial, global toll," *Tob Control* **21**(2), 87–91 (2012).
2. A. Churg et al., "Late intervention with a myeloperoxidase inhibitor stops progression of experimental chronic obstructive pulmonary disease," *Am. J. Respir. Crit. Care Med.* **185**(1), 34–43 (2012).
3. J. L. Wright et al., "Statin reverses smoke-induced pulmonary hypertension and prevents emphysema but not airway remodeling," *Am. J. Respir. Crit. Care Med.* **183**(1), 50–58 (2011).
4. S. Kobayashi et al., "A single dose of lipopolysaccharide into mice with emphysema mimics human chronic obstructive pulmonary disease exacerbation as assessed by micro-computed tomography," *Am. J. Respir. Cell Mol. Biol.* **49**(6), 971–977 (2013).
5. H. Parameswaran et al., "Three-dimensional measurement of alveolar airspace volumes in normal and emphysematous lungs using micro-CT," *J. Appl. Physiol. (1985)* **107**(2), 583–592 (2009).
6. M. Sasaki et al., "Evaluation of cigarette smoke-induced emphysema in mice using quantitative micro-computed tomography," *Am. J. Physiol. Lung Cell Mol. Physiol.* **308**(10), L1039–L1045 (2015).
7. E. G. Awji, J. C. Seagrave, and Y. Tesfaigzi, "Correlation of cigarette smoke-induced pulmonary inflammation and emphysema in C3H and C57Bl/6 mice," *Toxicol. Sci.* **147**(1), 75–83 (2015).
8. A. I. D'Hulst et al., "Time course of cigarette smoke-induced pulmonary inflammation in mice," *Eur. Respir. J.* **26**(2), 204–213 (2005).
9. A. Kemeny et al., "Integrative characterization of chronic cigarette smoke-induced cardio-pulmonary comorbidities in a mouse model," *Environ. Pollut.* **229**, 746–759 (2017).
10. Q. Li et al., "Integrative characterization of fine particulate matter-induced chronic obstructive pulmonary disease in mice," *Sci. Tot. Environ.* **706**, 135687 (2020).
11. M. G. Macowan et al., "Interventional low-dose azithromycin attenuates cigarette smoke-induced emphysema and lung inflammation in mice," *Physiol. Rep.* **8**(13), e14419 (2020).
12. G. Cao et al., "A dynamic micro-CT scanner based on a carbon nanotube field emission x-ray source," *Phys. Med. Biol.* **54**(8), 2323–2340 (2009).
13. N. L. Ford et al., "Prospective respiratory-gated micro-CT of free breathing rodents," *Med. Phys.* **32**(9), 2888–2898 (2005).
14. D. Cavanaugh et al., "In vivo respiratory-gated micro-CT imaging in small-animal oncology models," *Mol. Imaging* **3**(1), 55–62 (2004).
15. E. B. Walters et al., "Improved method of in vivo respiratory-gated micro-CT imaging," *Phys. Med. Biol.* **49**(17), 4163–4172 (2004).
16. C. Badea, L. W. Hedlund, and G. A. Johnson, "Micro-CT with respiratory and cardiac gating," *Med. Phys.* **31**(12), 3324–3329 (2004).
17. J. Hu et al., "Dynamic small animal lung imaging via a postacquisition respiratory gating technique using micro-cone beam computed tomography," *Acad. Radiol.* **11**(9), 961–970 (2004).
18. N. L. Ford et al., "Optimization of a retrospective technique for respiratory-gated high speed micro-CT of free-breathing rodents," *Phys. Med. Biol.* **52**(19), 5749–5769 (2007).
19. N. L. Ford et al., "Optimization of image quality in retrospective respiratory-gated micro-CT for quantitative measurements of lung function in free-breathing rats," *J. Biomed. Sci. Eng.* **07**(04), 157–172 (2014).

20. C. T. Badea et al., "4D micro-CT for cardiac and perfusion applications with view under sampling," *Phys. Med. Biol.* **56**(11), 3351–3369 (2011).
21. D. Ertel et al., "Respiratory phase-correlated micro-CT imaging of free-breathing rodents," *Phys. Med. Biol.* **54**(12), 3837–3846 (2009).
22. T. H. Farncombe, "Software-based respiratory gating for small animal conebeam CT," *Med. Phys.* **35**(5), 1785–1792 (2008).
23. N. L. Ford et al., "Quantifying lung morphology with respiratory-gated micro-CT in a murine model of emphysema," *Phys. Med. Biol.* **54**(7), 2121–2130 (2009).
24. X. Artaechevarria et al., "Evaluation of micro-CT for emphysema assessment in mice: comparison with non-radiological techniques," *Eur. Radiol.* **21**(5), 954–962 (2011).
25. A. Munoz-Barrutia et al., "Quantification of lung damage in an elastase-induced mouse model of emphysema," *Int. J. Biomed. Imaging* **2012**, 734734 (2012).
26. A. Tam et al., "Sex-related differences in pulmonary function following 6 months of cigarette exposure: implications for sexual dimorphism in mild COPD," *PLoS One* **11**(10), e0164835 (2016).
27. A. Tam et al., "Sex differences in airway remodeling in a mouse model of chronic obstructive pulmonary disease," *Am. J. Respir. Crit. Care Med.* **193**(8), 825–834 (2016).
28. N. L. Ford et al., "In vivo characterization of lung morphology and function in anesthetized free-breathing mice using micro-computed tomography," *J. Appl. Physiol. (1985)* **102**(5), 2046–2055 (2007).
29. N. Otsu, "A threshold selection method from gray-level histograms," *IEEE Trans. Syst., Man, Cybern.* **9**, 62–66 (1979).
30. C. C. Hsia et al., "An official research policy statement of the American Thoracic Society/European Respiratory Society: standards for quantitative assessment of lung structure," *Am. J. Respir. Crit. Care Med.* **181**(4), 394–418 (2010).
31. A. Churg, M. Cosio, and J. L. Wright, "Mechanisms of cigarette smoke-induced COPD: insights from animal models," *Am. J. Physiol. Lung Cell Mol. Physiol.* **294**(4), L612–L631 (2008).
32. S. Zhou et al., "Aging does not enhance experimental cigarette smoke-induced COPD in the mouse," *PLoS One* **8**(8), e71410 (2013).
33. N. L. Ford et al., "A respiratory-gated micro-CT comparison of respiratory patterns in free-breathing and mechanically ventilated rats," *Physiol. Rep.* **5**(2), e13074 (2017).

**Nancy L. Ford** received her PhD in medical biophysics from the University of Western Ontario. She is an associate professor in the Department of Oral Biological and Medical Sciences and the director of the UBC Centre for High-Throughput Phenogenomics. She is an associate member in the Department of Physics and Astronomy at the University of British Columbia (UBC). Her research interests include preclinical micro-CT and synchrotron imaging and clinical CBCT for medical and dental applications.

**Ian Lee** completed two co-op work terms in the Ford Lab as part of his degree in biotechnology (honours) from the UBC. Following graduation, he completed his nursing degree also from the UBC, and he is now employed as a registered nurse in Vancouver Coastal Health Authority in British Columbia.

**Julia Hwangbo** received her bachelor of science degree from the UBC in 2021. Her major was integrated sciences with a focus on neuroscience and genetics. During her undergraduate degree, she earned the Dean's honour list notation for three consecutive years, the science scholar notation in her final year, and graduated with high distinction. Currently, she is obtaining her master of occupational therapy degree at the University of Toronto.

**Anthony Tam** joined the team of Dr. Don Sin as a graduate student at the Center for Heart and Lung Innovation after graduating in biochemistry from UBC in 2009. Using preclinical models, he demonstrated sex-related differences in mucous and airway remodeling, which are two important clinical phenotypes of COPD. He used the genomics approach to identify candidate genes and lipid nanotechnology to elucidate the biology and treatment for age-related diseases.

**Don D. Sin** is the Director of the Centre for Heart Lung Innovation (HLI) and a professor of medicine at the UBC, Vancouver, Canada. He holds a Tier 1 Canada Research Chair in COPD and the De Lazzari Family Chair at HLI. His research focus is using "omics" data to discover innovative biomarkers of disease activity and new therapeutic targets to reduce hospitalization and mortality in patients with COPD.